The critical role of climate and saprolite weathering in landscape evolution

Jean L. Dixon,[1]* Arjun M. Heimsath[1] and Ronald Amundson[2]
[1] School of Earth and Space Exploration, Arizona State University, Tempe, AZ, USA
[2] Department of Environmental Science, Policy and Management, University of California, Berkeley, CA, USA

* Correspondence to: Jean L. Dixon, PSF 686, P.O. Box 871404, Tempe, AZ 85287-1404, USA. E-mail: jean.dixon@asu.edu

ESPL

Earth Surface Processes and Landforms

ABSTRACT: Landscapes evolve in response to external forces, such as tectonics and climate, that influence surface processes of erosion and weathering. Internal feedbacks between erosion and weathering also play an integral role in regulating the landscapes response. Our understanding of these internal and external feedbacks is limited to a handful of field-based studies, only a few of which have explicitly examined saprolite weathering. Here, we report rates of erosion and weathering in saprolite and soil to quantify how climate influences denudation, by focusing on an elevation transect in the western Sierra Nevada Mountains, California. We use an adapted mass balance approach and couple soil-production rates from the cosmogenic radionuclide (CRN) ^{10}Be with zirconium concentrations in rock, saprolite and soil. Our approach includes deep saprolite weathering and suggests that previous studies may have underestimated denudation rates across similar landscapes. Along the studied climate gradient, chemical weathering rates peak at middle elevations (1200–2000 m), averaging $112{\cdot}3 \pm 9{\cdot}7$ t km^{-2} y^{-1} compared to high and low elevation sites ($46{\cdot}8 \pm 5{\cdot}2$ t km^{-2} y^{-1}). Measured weathering rates follow similar patterns with climate as those of predicted silica fluxes, modeled using an Arrhenius temperature relationship and a linear relationship between flux and precipitation. Furthermore, chemical weathering and erosion are tightly correlated across our sites, and physical erosion rates increase with both saprolite weathering rates and intensity. Unexpectedly, saprolite and soil weathering intensities are inversely related, such that more weathered saprolites are overlain by weakly weathered soils. These data quantify exciting links between climate, weathering and erosion, and together suggest that climate controls chemical weathering via temperature and moisture control on chemical reaction rates. Our results also suggest that saprolite weathering reduces bedrock coherence, leading to faster rates of soil transport that, in turn, decrease material residence times in the soil column and limit soil weathering. Copyright © 2009 John Wiley & Sons, Ltd.

KEYWORDS: climate; saprolite; chemical weathering; cosmogenic radionuclides; erosion

Introduction

Regolith, including soil and saprolite, mantles much of the continental surface and plays an integral role in ecosystem function by providing biological substrates, influencing water partitioning across the landscape and acting as the source and site of denudation processes like erosion and chemical weathering. On hillslopes, soils provide a critical interface between the atmosphere and land surface, and therefore have become the focus for studies examining links between climate, erosion and weathering (White and Blum, 1995; Riebe *et al.*, 2001a; Millot *et al.*, 2002; von Blanckenburg, 2006). Climate is thought to influence landscape evolution by its control on erosion and weathering processes. Laboratory experiments and modeling approaches that tackle links between climate and chemical weathering indicate temperature and water availability influence rates of chemical reactions (White *et al.*, 1999; White and Brantley, 2003), and several studies based on field measurements have reported predictable patterns of watershed chemical weathering with climate, such that wetter or warmer sites experience faster rates of weathering (e.g. White and Blum,

1995; Stewart *et al.*, 2001; Riebe *et al.*, 2003b). Links between climate and physical erosion are more elusive, and few field-based studies have shown clear relationships between climate variables and erosion rates, leading some authors to suggest climate exerts only minimal control on rates of landscape evolution (Riebe *et al.*, 2001a; von Blanckenburg, 2006).

Clear mechanisms link climate and chemical weathering. Temperature influences weathering through kinetic controls on the rate of chemical reactions. Water removes dissolved material from rock and soil and affects what reactions occur. Measured chemical weathering rates reflect the combined effects of temperature and precipitation. These effects can be difficult to disentangle and may obscure the relationship between climate and weathering, especially along orographic gradients where temperature and precipitation variations have competing effects on weathering rates. To understand the role climate forcing plays in controlling chemical weathering, combined effects of temperature and precipitation on chemical fluxes have been previously modeled by coupling an Arrhenius equation and theorized linear or power-law effects of precipitation (e.g. White and Blum, 1995):

$$Q_i = (a_i * P) * e^{\left[\frac{-E_a}{R}\right]\left[\frac{1}{T} - \frac{1}{T_0}\right]} \qquad (1)$$

Here, Q_i is the chemical flux of an element 'i' (in mol ha^{-1} y^{-1}), a_i is a correlation coefficient between precipitation and element flux, E_a is the activation energy (in kJ mol^{-1}), R is the gas constant, P is the precipitation (in mm y^{-1}), T is air temperature and T_0 is a reference temperature (in degree Celsius). This function describes a linear relationship between precipitation and weathering flux, however the slope of this relationship increases exponentially with increasing temperature. Similarly, the temperature-weathering relationship is enhanced by precipitation. The resulting model predicts accelerated weathering where precipitation and temperature are both high, and retarded weathering in regions of low precipitation and/or low temperatures. Using this function, White and Blum (1995) identified independent controls on silica fluxes by temperature and precipitation in granitic basins distributed worldwide.

In addition to direct temperature and water-availability controls on rates of weathering reactions, flora and fauna are heavily influenced by climate and play an important role in both physical transport and weathering processes in soils. Biota actively transport and mix soil through tree throw, bioturbation, and root disruption (Heimsath et al., 2001), and can further influence erosion through resistance to overland flow and maintenance of steep hillslopes (Collins et al., 2004). Biotic mixing also influences soil porosity, bulk density, and water infiltration, which further impact weathering processes in soils (Brimhall et al., 1992). Precipitation and temperature directly affect weathering reactions; however, links between climate and erosion are not as straightforward. The amount of precipitation or average temperatures may influence the efficacy of soil transport by overland flow or soil creep following freeze–thaw, tree-throw or raindrop splash (Tucker and Slingerland, 1997; Hales and Roering, 2007). Dominant mechanisms of sediment production and transport are not uniform across all landscapes, potentially obscuring direct quantifiable links between erosion rates and climate.

Despite uncertainty in how erosion and weathering respond to external forcings, a range of studies have shown internal positive feedbacks between erosion and weathering rates (Anderson et al., 2002; Millot et al., 2002; Jacobson et al., 2003; Riebe et al., 2004; West et al., 2005; Fletcher et al., 2006). Erosion provides fresh mineral surfaces for chemical weathering reactions. Similarly, chemical weathering can assist erosion through dissolution of primary minerals, thereby reducing bedrock coherence and resistance to physical disruption. This coupling has led some to suggest that physical erosion exerts a strong control on chemical weathering (Riebe et al., 2001b; von Blanckenburg, 2006).

Most studies that examine controls on chemical weathering and erosion, by both internal and external forces, focus on the soil system. Chemical weathering in saprolite, the weathered parent material retaining relict rock structure and lying beneath mobile soil, may meet or exceed rates of soil weathering in upland landscapes such as the central and southern Appalachians (Stolt and Baker, 2000), the Oregon Coast range (Anderson et al., 2002), southeastern Australia (Green et al., 2006; Burke et al., 2007), Puerto Rico (Riebe et al., 2003a) and the Sierra Nevada (Dixon et al., 2009), suggesting saprolite weathering plays an integral role in landscape evolution. Saprolite has been studied in depth for its geochemical properties (Pavich, 1990; White et al., 1998; Price et al., 2005; Lebedeva et al., 2007), and studies of saprolite weathering typically focus on secondary mineral development (Nesbitt and Markovics, 1997; White et al., 2001) or grain-scale geochemical transformations (Murphy et al., 1998; Nugent et al., 1998). These small-

scale transformations play an important role in how the saprolite system influences physical and chemical processes in the overlying soil system, and numerous authors have noted the likely importance of deep weathering to denudation and landscape relief (Büdel, 1957; Ollier, 1960; Thomas, 1966, 1994; Migoń and Lidmar-Bergström, 2001; Phillips, 2005). Lidmar-Bergström (1995) suggested that the stripping of deep saprolite weathering mantles has played a fundamental role in relief differentiation within the Baltic Shield, and Migoń and Alcántara-Ayala (2008) highlighted connections between the formation of weathered granite, uplift rate and the processes of slope lowering in mountainous regions of Mexico. Despite the central importance saprolite weathering may play in landscape evolution, a quantitative consideration of saprolite geochemistry is rarely factored into studies of landscape geomorphology (e.g. Pavich, 1986) and few studies have explicitly accounted for saprolite weathering (Anderson et al., 2002; Burke et al., 2007) in quantifying feedbacks between erosion and weathering. Our understanding of the controlling factors of landscape evolution is therefore incomplete, due to both limited field data on soil weathering and erosion and a noticeable lack of studies that measure saprolite weathering.

Here, we examine the largely unquantified role of saprolite in influencing landscape evolution and hillslope form. We measured rates of physical erosion and both soil and saprolite chemical weathering along a western Sierra Nevada climate gradient to examine external climate controls on landscape evolution and internal feedbacks between erosion and weathering. We adapted a mass balance approach from Riebe et al. (2003a) that relies on the assumption of steady state regolith thickness and uses ^{10}Be concentrations in saprolite and zirconium concentrations in rock, saprolite and soil to calculate rates of soil production, erosion and weathering. The results help quantify climate controls on the long-term evolution of upland landscapes through saprolite weathering.

Conceptual Framework for Quantifying Erosion and Weathering

Consider a depth-profile at a hillcrest, extending from the soil surface to unweathered bedrock (Figure 1). The layer of physically and/or chemically altered material (saprolite and soil) atop crystalline bedrock can be millimeters to tens of meters thick on different landscapes. A number of definitions are found throughout the literature for these terms; here, 'soil' is the physically mobile material that is produced by the mechanical disruption of the underlying bedrock (Figure 1a) or saprolite (Figure 1b), and 'saprolite' is the non-mobile, deep weathering mantle produced by chemical alteration and dissolution of the bedrock. At the upper boundary, saprolite is incorporated into the mobile soil column through physical disruption by soil production mechanisms such as tree throw, bioturbation, and frost cracking. At the lower boundary, saprolite is produced from parent bedrock by chemical dissolution and mineral transformation. While mineralogical changes and alteration occurs throughout the saprolite column, much of the chemical mass loss can occur as a discrete weathering front near the bedrock boundary (Frazier and Graham, 2000; Buss et al., 2004; Fletcher et al., 2006; Lebedeva et al., 2007; Buss et al., 2008). In this paper, we focus on the mass loss due to chemical processes (here termed chemical weathering) and physical processes (here termed erosion) on soil mantled hillslopes. By these definitions, weathering within saprolite is purely chemical, while soils evolve by both chemical transformations and physical disruption and erosion.
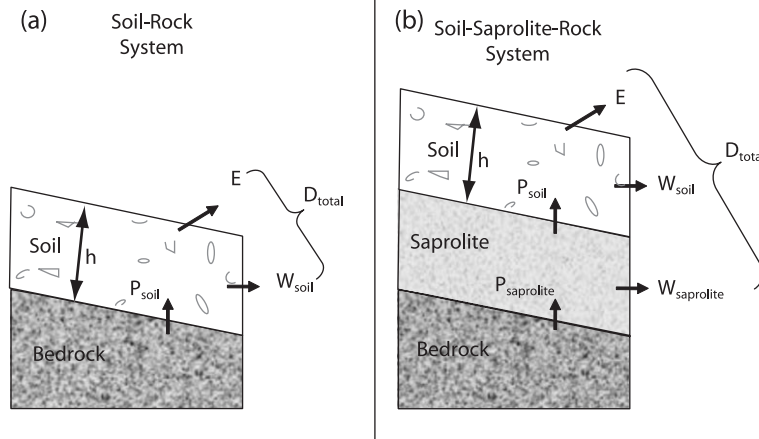
Figure 1. Theoretical Framework for soil and saprolite. Soils may be mechanically produced from bedrock (a) or weathered saprolite (b). Based on conservation of mass Equations 2 and 3, if soils have a steady state thickness, then soil production (P_{soil}) is balanced by weathering (W_{soil}) and erosion (E). If saprolite thickness attains a similar steady state, then saprolite production (P_{sap}) is balanced by mass loss from the saprolite profile by weathering (W_{sap}) and the mechanical conversion to soil (P_{soil}). Note that total denudation rate (D_{total}) is calculated from the sum of losses, and reflects only erosion and weathering in soil in Figure 1a, but accounts for the additional losses due to saprolite weathering in Figure 1b.

According to mass conservation, any change in soil mass, expressed as the product of soil density (ρ_{soil}) and change in soil thickness (h), reflects rates of soil production (P_{soil}), erosion (E) and weathering (W_{soil}), such that:

$$\rho_{soil} \frac{\partial h}{\partial t} = P_{soil} - E - W_{soil} \qquad (2)$$

where rates are in ton km^{-2} y^{-1}. If soil thickness (h) is constant over time ($\frac{\partial h}{\partial t} = 0$), then the rate of soil mass loss equals the rate of soil production:

$$P_{soil} = E + W_{soil} \qquad (3)$$

The sum of all rates of mass loss can be termed the total denudation rate (D_{total}), and these losses occur by physical erosion of soil and chemical weathering in both the soil (W_{soil}) and the saprolite (W_{sap}), such that (Figure 1b):

$$D_{total} = E + W_{total} = E + W_{soil} + W_{sap} \qquad (4)$$

Recalling mass conservation for steady state soil thickness (Equation 3), Equation 4 can be written:

$$D_{total} = P_{soil} + W_{sap} \qquad (5)$$

It is important to note from Equation 5 that the soil production rate (P_{soil}) is smaller than the total denudation rate (D_{total}) in a landscape that experiences chemical weathering in the saprolite. Furthermore, I$_{soil}$, which represents a rate of mass flux, can be converted to a landscape lowering rate in units of length per time by dividing by saprolite density. Thus D_{total} cannot as easily be converted into a lowering rate because of its associated saprolite weathering term in Equation 5; saprolite weathering is likely isovolumetric, and mass is lost from the saprolite without a corresponding change in volume.

Rates of chemical weathering in catchments have commonly been quantified using stream solute data. These measurements provide a valuable quantification of instantaneous weathering, but provide limited insight into landscape evolution due to their short measurement time scales (1–10 years) and because they integrate mass losses from all points within the catchment, thus treating a watershed as a black box. Riebe *et al.* (2003a) developed a method to calculate chemical weathering rates

in actively eroding terrains by coupling a mass balance approach using immobile elements (Brimhall and Dietrich, 1987) to rates of landscape lowering derived from cosmogenic radionuclides (CRNs). CRNs such as [10]Be and [26]Al provided a tool to measure surface rates of denudation over longer time scales (10^3–10^5 years) than solute measurements (1–10 years). These longer time scales, though still only a fraction of the evolutionary period of some landscapes, are more relevant to studies examining the influence of external forcing (climate and tectonics) on landscape change.

CRN concentrations in a sample of rock, saprolite or soil record the rate of surface denudation processes that removed overlying mass, and therefore the rate at which the sample approaches the land surface (Lal, 1991):

$$D_{CRN} = \frac{P_0 \Lambda}{N} \qquad (6)$$

Here, the surface denudation rate (D_{CRN}; in g cm^{-2} y^{-1}) is a function of the measured CRN concentration in quartz (in atoms g^{-1}), the CRN production rate at the surface (P_0: in atoms g^{-1} y^{-1}), which decreases exponentially with depth, and the CRN attenuation length (Λ; in g cm^{-2}). A complete version of Equation 6, used to calculate rates in this paper, is presented and discussed thoroughly by Balco *et al.* (2008); however, the simplified version shown by Equation 6 is sufficient for the purposes of our discussion. For [10]Be, the most widely used CRN for determining landscape denudation rates, the penetration depths of cosmic rays, assuming a mean attenuation of 160 cm^2 kg^{-1}, are ~140 cm through soil and ~60 cm through rock (Balco *et al.*, 2008). Nuclide concentrations, therefore, record near-surface mass removal within the top couple of meters of the Earth's surface, and therefore will reflect both chemical and physical losses within soil (typically less than 2 m thick); however, mass losses due to chemical weathering at the bedrock-saprolite boundary are likely to occur at deeper depths than recorded by CRNs. A sample of soil, saprolite or rock will, therefore, have a [10]Be concentration that reflects the rate at which overlying soil was removed. Assuming local steady state soil thickness (Equation 3), this rate is equivalent to the soil production rate (Heimsath *et al.*, 1997, 1999; Heimsath, 2006):

$$D_{CRN} = P_{soil} \qquad (7)$$

Here, we caution that the generic term denudation (D_{total}) should not be used to specifically denote CRN-derived rates of landscape lowering. CRN-derived rates do not capture the result of deep saprolite weathering, and thus only record a portion of total denudation on deeply weathered landscapes. As a consequence, we distinguish between soil production rates (P_{soil}) that equal CRN-derived surface denudation rates (D_{CRN}), and total denudation rates (D_{total}) that reflect combined rates of mass loss in soil and saprolite due to physical and chemical processes. To fully quantify the potential mass loss from deep saprolite chemical weathering we expand upon previously developed methods for determining soil production, erosion and chemical weathering rates.

The enrichment of an immobile element in a weathered product relative to the parent material can be used to calculate the fraction of mass that was lost to chemical weathering (Brimhall and Dietrich, 1987). Riebe (2001b) termed this relationship the chemical depletion fraction (CDF):

$$CDF = \left(1 - \frac{[I]_p}{[I]_w}\right) \qquad (8)$$

where the subscripts 'p' and 'w' refer to concentrations of the immobile element (I) in the parent material and weathered material, respectively. For accurate calculation of the CDF, several important conditions must be met: homogeneous parent material; chemical immobility of the reference element (e.g. zirconium, Zr); and minimal chemical weathering during lateral soil transport. We explore these conditions in the last section of the Discussion.

Equation 8 can be used to represent the chemical depletion fraction due to soil weathering, saprolite weathering, or total weathering processes. We term these respective depletions fractions the CDF_{soil}, CDF_{sap} and CDF_{total}:

$$CDF_{soil} = \left(1 - \frac{[Zr]_{saprolite}}{[Zr]_{soil}}\right) \qquad (9)$$

$$CDF_{saprolite} = \left(1 - \frac{[Zr]_{rock}}{[Zr]_{saprolite}}\right) \qquad (10)$$

$$CDF_{total} = \left(1 - \frac{[Zr]_{rock}}{[Zr]_{soil}}\right) \qquad (11)$$

In Equations 9–11, we have replaced the generic immobile element 'I', with the element zirconium, which is immobile in most weathering environments (e.g. Green et al., 2006).

Following Riebe et al. (2003a), the total chemical weathering rate is the product of the total denudation rate and the total CDF:

$$W_{total} = D_{total} * \left(1 - \frac{[Zr]_{rock}}{[Zr]_{soil}}\right) = D_{total} * CDF_{total} \qquad (12)$$

Here, the CDF_{total} represents the fraction of total denudation (D_{total}) that occurs by all chemical losses (in both the saprolite and the soil). Assuming steady state soil and saprolite thickness, the saprolite weathering rate is:

$$W_{sap} = D_{total} * \left(1 - \frac{[Zr]_{rock}}{[Zr]_{sap}}\right) = D_{total} * CDF_{saprolite} \qquad (13)$$

and the soil weathering rate is the calculated difference between W_{total} and W_{sap}:

$$W_{soil} = W_{total} - W_{sap} \qquad (14)$$

Calculations of chemical weathering and erosion rates require the measurement of CRN-derived soil production rates. Taking this into account, we rearrange the equations for erosion and weathering in terms of CRN-derived P_{soil} (Equation 6). The weathering rate of soil (W_{soil}) is calculated as the product of P_{soil} and the CDF_{soil}:

$$W_{soil} = P_{soil} * \left(1 - \frac{[Zr]_{saprolite}}{[Zr]_{soil}}\right) = P_{soil} * CDF_{soil} \qquad (15)$$

Here, the CDF_{soil} represents the fraction of original saprolite mass lost due to chemical weathering. The erosion rate (E), can then be calculated as the difference between P_{soil} and W_{soil} following Equation 3):

$$E = P_{soil} - W_{soil} \qquad (16)$$

Lastly, the rate of saprolite weathering (W_{sap}) is calculated by returning to basic principles regarding conservation of mass for immobile elements. For a chemically immobile element such as zirconium, the conservation of mass equation can be written:

$$P_{sap} * [Zr]_{rock} = P_{soil} * [Zr]_{saprolite} = E * [Zr]_{soil} \qquad (17)$$

Here, P_{sap} (Figure 1b) represents the rate conversion of rock to saprolite, and is mathematically equivalent to the total denudation rate (D_{total}) assuming a steady state regolith thickness. Solving for total denudation yields:

$$D_{total} = P_{sap} = P_{soil}\left(\frac{[Zr]_{saprolite}}{[Zr]_{rock}}\right) \qquad (18)$$

Substituting Equation 18 into Equation 13 then gives us the equation for the saprolite weathering rate (W_{sap}):

$$W_{sap} = P_{soil} * \left(\frac{[Zr]_{saprolite}}{[Zr]_{rock}} - 1\right) \qquad (19)$$

Summing calculated weathering and erosion rates from Equations 15, 16 and 19 allows one to calculate the total denudation rates (Equation 4). These equations differ from those of Riebe et al. (2003a) by the definition that CRN derived rates reflect only soil production rates, and not total denudation rates in regions mantled by saprolite. We explore this distinction and its implications in our discussion. We use this adapted mass balance approach to calculate rates of erosion and weathering in the Sierra Nevada to explore the role of climate on erosional and weathering processes.

Study Site and Methods

This study is located along an elevational (climate) gradient in the western Sierra Nevada range of California. The transect is ~64 km long, extending from the low elevation grasslands near Fresno, California (~200 m above sea level) to subalpine forests at Kaiser Pass (~3000 m elevation), the first expression of the Sierran crest in this region. Precipitation increases from
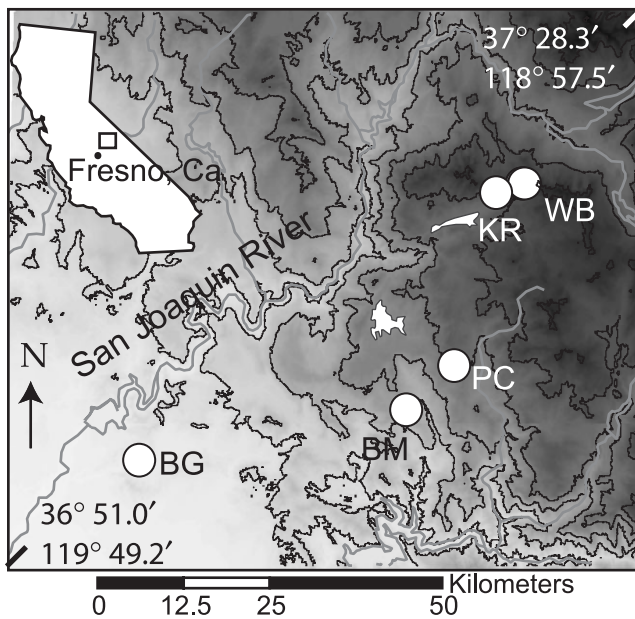
Figure 2. Study sites follow an elevation transect up the western front of the Sierra Nevada (200–3000 m elevations). The low elevation site BG is located approximately 40 km northwest from Fresno, California. Sites fall within the San Joaquin and Kings River Drainages, and occupy distinct climate zones. Regional topography is shown by 500 m shaded elevation contours.

33–127 cm and mean annual temperature decreases from 16·7 °C to 3·9 °C (Prism-Database) with increasing elevation. These patterns result in distinct changes in floral communities with elevation. We examined five study sites within different climate zones along the transect (Table I; Figure 2): Blasingame (BG), at 220 m in the oak-grassland zone; Bretz Mill (BM) at 1220 m in the lower mixed-conifer zone; Providence Creek (PC) at 1980 m in the upper mixed-conifer zone; Kaiser Road (KR) at 2680 m in the conifer-subalpine transition zone; and Whitebark (WB) at 2990 m in the subalpine Canadian zone.

All the hillslopes are underlain by granitic rocks and are on unglaciated terrain based on topography, field observations, US Geological Survey geomorphology maps, and the presence of saprolite at high elevations where glaciations would have otherwise removed it. All slopes are soil mantled, and soil depths across all sites range from 6 to 127 cm, averaging 67 ± 5 cm standard error. All sites except one (KR) have saprolite. Limited roadcuts showed that saprolite thickness exceeds 10 m at the middle elevation sites BM and PC; however we were unable to estimate this thickness at other sites. We found little evidence of landsliding, which would have complicated measurements of soil depth and the soil production rates determined from cosmogenic [10]Be data. Field observations suggest that soil transport on these hillslopes likely occurs by a combination of creep-like processes and overland flow. Average hillslope gradients throughout the region are ~12°.

Previous research along the transect has focused on soil morphology and chemistry on gentle backslopes, and on the carbon cycling rates in these soils (Dahlgren *et al.*, 1997; Trumbore *et al.*, 1996). Dahlgren *et al.* (1997) showed a systematic change in clay concentrations and clay mineralogy with increasing elevation, with the highest soil clay content (535·8 kg m^{−2}) occurring in middle elevation sites (~1200–2000 m), suggesting greater chemical weathering at intermediate elevations. The bedrock in the region has been extensively studied, and some chemical and mineralogical data is available

for bedrock (Bateman and Busacca, 1983; Bateman and Lockwood, 1970, 1976).

The Sierra Nevada range is an ideal location to examine links between erosion, chemical weathering and climate because variations in other factors that strongly influence soil development (e.g. Jenny, 1941), such as tectonics (topography and time) and lithology (parent material), are minimal. The timing and magnitude of late Cenozoic uplift in the Sierras is still debated; however, much of the upland soil-mantled landscape has not yet responded to tectonic forcings in recent times. Helium thermochronometry (e.g. Clark *et al.*, 2005) and CRN-dated cave sediments (Stock *et al.*, 2004) suggest rapid river incision in the western Sierra Nevada is likely associated with late Cenozoic uplift, however oxygen isotope data in soil carbonates in the shadow of the eastern Sierra Nevada (Poage and Chamberlain, 2002) suggest persistent relief dating back to middle Miocene. Longitudinal stream profiles across the western front of the range show a low-relief 'relict' landscape separated from incising canyons by river knickpoints (Riebe *et al.*, 2000; Clark *et al.*, 2005; Cecil *et al.*, 2006), and CRN-derived rates of denudation in the upland soil-mantled region average 30–40 m My[−1] (this study; Small and Anderson, 1995; Riebe *et al.*, 2001a); these rates approximate the longer term denudation determined from He thermochronology (House *et al.*, 1998) and are considerably lower than tectonically driven incision rates of ~200 m My[−1] (Stock *et al.*, 2004). In summary, we consider that the upland hillslopes selected for our study sites have all experienced the same minimal tectonic and glacial influences on denudation, and that erosion and weathering rates have achieved a local steady state with respect to the present climatic regimes.

Following Dahlgren *et al.*'s (1997) study of soil thickness and chemistry with elevation, we selected hillslopes within each climate zone and excavated soil pits approximately every 20 m along downslope transects to sample saprolite beneath soil for cosmogenic [10]Be analyses. Soil samples of known volume were collected by push core, dried at 115 °C for 48 hours, and weighed for bulk density analysis. We collected additional bulk soil samples from soil pits for trace element chemistry. These samples were oven dried and homogenized by pulverizing in a tungsten carbide mill to less than 250 μm; we sub-sampled approximately 20–40 g of pulverized sample for analysis by X-ray fluorescence (XRF). We measured zirconium concentrations by pressed pellet XRF at Keene State University (New Hampshire) and ALS-Chemex commercial laboratories (Reno, Nevada).

For each location on a hillslope, we used zirconium concentrations to calculate the chemical weathering intensity in soils and saprolites (Equations 9–11). Combining measured zirconium concentrations (Table II) with soil production rates from [10]Be concentrations (Table III), we calculated chemical weathering rates of soils (Equation 15) and saprolites (Equation 19), and physical erosion rates (Equation 16). We compared patterns of measured weathering rates across our climate zones to predicted silica fluxes modeled in Equation 1 (White and Blum, 1995).

Results

Rates of local soil production, calculated from [10]Be concentrations, vary from 31 to 136 t km^{−2} y[−1] (Table III). Using an average measured saprolite bulk density of 2·2 g cm^{−3}, these soil production rates correspond to landscape lowering rates of 14 to 62 m My[−1]. We report rates in terms of mass flux rather than length per time due to uncertainties in saprolite density. Rates of soil weathering and physical erosion on hillslopes

Table I. Descriptions of sites and climate zones

Site	Location (deg)	Elevation (m)	Climate zone	MAP[a] (cm y^{-1})	MAT[a] (°C)	Bedrock[b]	Erosion processes[c]	Soil description[d]	Saprolite description
Blasingame (BG)	36·9535–119·6308	216	Oak-Grassland	37	16·6	Blue Canyon Tonalite	Soil creep by pocket gopher bioturbation	Coarse-loamy, mixed, thermic; Typic Xerochrept	Granular; clear rock fabric
Bretz Mill (BM)	37·0390–119·2548	1186	Low Mixed-Conifer	77	12	Dinky Creek Granodiorite	Soil creep by tree throw	Fine-loamy-mixed, mesic; Ultic Haploxeralf	Clay- and silt-rich; Obscure rock fabric
Providence Creek (PC)	37·0652–119·2055	1952	Upper Mixed Conifer	92	8·9	Dinky Creek Granodiorite	Soil creep by tree throw	Sandy, mixed, mesic; Pachic Xerumbrept	Sandy; moderately clear rock fabric with granular clasts
Kaiser Road (KR)	37·2833–119·1068	2681	Conifer – Subalpine Transition	106	4	Mount Givens Granodiorite	Overland flow; Soil creep by bioturbation and tree throw	Sandy-skeletal, mixed; Entic Cryumbrept	No saprolite; soils underlain by fractured bedrock
Whitebark (WB)	37·2823–119·0875	2991	Subalpine/Canadian	106	3·9	Mount Givens Granodiorite	Overland flow; Soil creep by pocket gopher bioturbation	Sandy-skeletal, mixed; Entic Cryumbrept	Granular; clear rock fabric; Some bedrock clasts

[a] Mean annual precipitation (MAP) and mean annual temperature (MAT) obtained from the Prism Group at Oregon State University (Prism-Database).
[b] Bedrock previously mapped in the region by Bateman and Busacca (1983) and Bateman and Lockwood (1970, 1976).
[c] Erosion processes determined from field observations and Dixon et al. (2009).
[d] Soil types from Dahlgren et al. (1997).

Table II. Zirconium concentrations and CDFs of soil and saprolite

Sample	Distance from crest (m)	$[Zr]_{soil}$ (ppm)	$[Zr]_{saprolite}$ (ppm)	CDF_{soil} (%)	CDF_{sap}[b] (%)	CDF_{total} (%)	$1 - CDF_{total}$ (%)
Blasingame[a]							
LD-0	0	120	130	0	53	50	50
LD-1	20	103	111	0	45	41	59
LD-2	40	105	81	23	25	42	58
LD-3	60	129	64	50	5	53	47
LD-4	80	134	79	41	23	55	45
LD-5	100	130	81	38	25	53	47
LD-6	120	139	124	11	51	56	44
	Mean ± standard error (SE)			20 ± 6	40 ± 7	54 ± 3	46 ± 3
Bretz Mill[a]							
BM-1	0	n.d.	125	n.d.	37	n.d.	n.d.
BM-2006-1	5	124	154	0	49	37	63
BM-2006-2	30	147	118	20	34	47	53
BM-2006-3	40	147	130	12	40	47	53
BM-2006-4	60	155	114	27	31	50	50
	Mean ± SE			18 ± 5	35 ± 5	45 ± 2	55 ± 2
Providence Creek[a]							
PC-1	0	135	131	3	54	55	45
PC-2006-4	20	154	115	25	47	61	39
PC-2006-3	40	144	146	0	58	58	42
PC-2006-2	60	139	147	0	59	56	44
PC-2006-1	80	149	152	0	60	59	41
PC-2	100	143	117	18	48	58	42
	Mean ± SE			8 ± 5	54 ± 2	58 ± 1	42 ± 1
Kaiser Road[a]							
KR-1	0	n.d.	114	n.d.	13	n.d.	n.d.
KR-2	20	n.d.	99	n.d.	0	n.d.	n.d.
KR-2006-1	40	145	129	11	23	32	68
KR-2006-3	60	152	135	12	26	35	65
KR-2006-4	80	155	n.d.	n.d.	n.d.	36	64
	Mean ± SE			11 ± 2	16 ± 6	34 ± 1	66 ± 1
Whitebark[a]							
WB-0	0	182	148	18	36	48	52
WB-1	20	185	154	17	38	49	51
WB-2	40	168	215	0	56	43	57
WB-3	60	180	95	47	0	47	53
WB-4	80	178	155	13	39	47	53
WB-5	100	223	126	44	25	57	43
WB-6	120	166	112	32	15	43	57
WB-7	140	234	142	40	33	59	41
WB-8	160	160	138	14	31	41	59
	Mean ± SE			25 ± 5	30 ± 5	48 ± 2	52 ± 2

[a] Rock [Zr] measured from exposed tor or bedrock beneath soil at each site: BG (61 ppm), BM (78 ppm), PC (61 ppm), KR (99 ppm), WB (95 ppm).
[b] Where saprolite [Zr] exceeds soil concentrations, saprolite CDF would be negative. In these, we adjust CDF_{sap} to zero.

average $14 \cdot 7 \pm 2 \cdot 5$ t km^{-2} y^{-1} and $67 \cdot 4 \pm 6 \cdot 3$ t km^{-2} y^{-1} (mean ± standard error, $n = 29$), respectively (Table IV). Saprolite weathering rates average $53 \cdot 5 \pm 8 \cdot 4$ t km^{-2} y^{-1} ($n = 31$), almost a factor of four higher than weathering in overlying soil. Total denudation rates exhibit a wide range of values across the hillslopes and climate zones, from 36 to 295 t km^{-2} y^{-1}, with a mean of $133 \cdot 8 \pm 13 \cdot 2$ t km^{-2} y^{-1}.

The CRN-based erosion rates are positively correlated with total weathering ($r^2 = 0 \cdot 69$, Figure 3a) and saprolite weathering rates ($r^2 = 0 \cdot 65$, Figure 3b). Erosion rates increase from 24 to 132 t km^{-2} y^{-1} as weathering rates increase from 18 to 173 t km^{-2} y^{-1}. There is no evidence for a positive relationship between physical erosion and soil weathering rates (Figure 3c). Also, the physical erosion rates do not vary predictably with total weathering as reflected by the CDF_{total}, which cluster near an average value of 0·5, equivalent to a 50% chemical depletion (Figure 4a; Table II). Data from CDF_{total} indicate that an average of half of the total denudation on these hillslopes is accomplished by chemical weathering. Our data show a weak positive relationship between physical erosion rates and CDF_{sap} ($r^2 = 0 \cdot 27$, $n = 29$; Figure 4b), and a negative relationship between erosion and CDF_{soil} ($r^2 = 0 \cdot 30$, $n = 29$; Figure 4c). The intensity of chemical weathering in soils and saprolites are inversely related (Figure 5); as saprolite weathering (CDF_{sap}) increases from 0 to 60%, CDF_{soil} decreases from 0 to 50% ($r^2 = 0 \cdot 69$, $n = 29$).

Denudation rates vary at a local scale across individual hillslopes and at a landscape scale across the climate gradient; rates of chemical weathering and physical erosion are generally highest in the middle climate zones, PC and BM, between 1200 and 2000 m elevation (Figures 6a–6c). At these elevations, physical erosion and total chemical weathering rates average

**Table III.** Data for derivation of cosmogenic [10]Be soil production rates

Sample	[10]Be concentration (atoms/g)[a]	Sample depth (cm)	Depth shielding factor[b]	Topo shielding factor[b]	Soil production rate[c] (t km^{-2} y^{-1})
LD-0	187403 ± 34399	6	0·96	1·00	66·2 ± 14·4
LD-1	90282 ± 3745	25	0·80	0·99	126·4 ± 9·9
LD-2	107038 ± 7076	27	0·82	0·99	104·9 ± 10·1
LD-3	132701 ± 5745	40	0·70	1·00	69·2 ± 5·5
LD-4	93307 ± 2265	45	0·67	1·00	93·3 ± 6·4
LD-5	136789 ± 4587	53	0·62	1·00	59·8 ± 4·4
LD-6	131622 ± 5941	75	0·51	0·99	51·2 ± 4·2
BM-2006-1	139642 ± 6250	91	0·51	1·00	89·5 ± 7·5
BM-2006-2	112402 ± 4826	74	0·59	1·00	128·5 ± 10·6
BM-2006-3	81255 ± 4697	102	0·48	1·00	148·5 ± 13·7
BM-2006-4	85036 ± 3858	127	0·40	1·00	117·4 ± 9·8
PC-01 sap	142131 ± 3515	80	0·51	1·00	136·0 ± 10·6
PC-2006-4	267476 ± 7295	71	0·60	1·00	84·3 ± 6·7
PC-2006-3	200316 ± 5981	61	0·64	1·00	122·7 ± 9·9
PC-2006-2	213394 ± 6733	91	0·51	1·00	92·3 ± 7·5
PC-2006-1	214359 ± 7237	107	0·46	1·00	82·0 ± 6·7
PC-02 sap	235228 ± 5730	110	0·46	0·99	72·5 ± 5·7
KR-1	1299981 ± 37499	33	0·74	0·99	31·2 ± 2·7
KR-2	606252 ± 29298	25	0·83	0·99	77·4 ± 7·2
KR-2006-1	619532 ± 30456	64	0·63	1·00	58·0 ± 5·4
KR-2006-1[d]	607500 ± 23068	64	0·63	1·00	59·2 ± 5·2
KR-2006-3	765999 ± 24034	64	0·63	1·00	46·6 ± 4·0
WB-0-R	581657 ± 17376	53	0·61	1·00	70·5 ± 6·0
WB-1-R	578575 ± 48527	64	0·55	1·00	65·1 ± 7·6
WB-2-R	801896 ± 32260	70	0·52	1·00	34·2 ± 3·1
WB-3-R	367081 ± 13488	110	0·35	1·00	66·1 ± 5·8
WB-4-R	824462 ± 19688	75	0·49	1·00	40·2 ± 3·4
WB-5-R	688245 ± 18081	75	0·50	1·00	48·7 ± 4·1
WB-6-R	1081770 ± 25628	60	0·57	0·99	35·0 ± 3·0
WB-7-R	406837 ± 13257	90	0·43	0·98	71·4 ± 6·1
WB-8-R	789064 ± 30516	80	0·47	1·00	40 ± 3·6

[a] [10]Be concentrations measured by accelerator mass spectrometry at Lawrence Livermore and Perdue Laboratories.
[b] Topographic shielding factor calculated from strike/dip measurements and applied to muogenic and spallogenic [10]Be production. Depth correction applied only to spallogenic production.
[c] Rates calculated assuming constant [10]Be production following Balco *et al.* (2008).
[d] Two separate samples of KR-2006-1 were run. Weathering and erosion rates in Table IV are calculated using the average soil production rate.
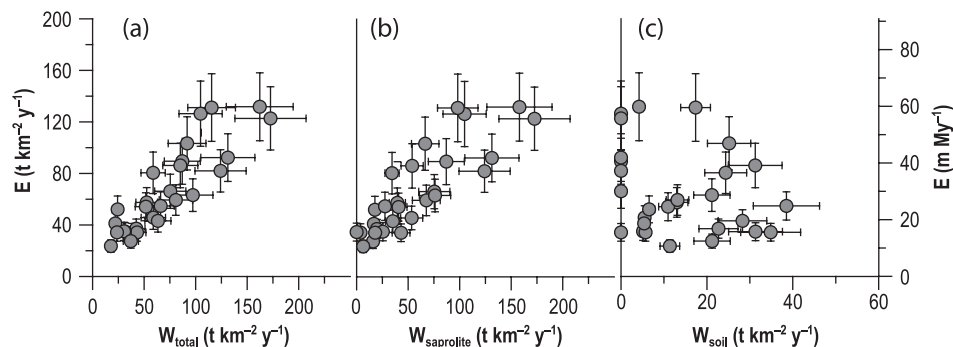
Figure 3. Physical erosion rates increase with total weathering (a) and saprolite weathering (b) rates, however links with soil weathering (c) are not as clear. Linear regressions suggest strong links between erosion rates and both total and saprolite weathering rates ($r^2 = 0.69$ and 0.65 respectively).

97·6 ± 7·5 t km^{-2} y^{-1} and 112·3 ± 9·7 t km^{-2} y^{-1} ($n = 11$), respectively, which is much higher than average rates in the other climate zones (49·0 ± 5·7 and 46·8 ± 5·2 t km^{-2} y^{-1}) ($n = 18$). Modeled silica fluxes, calculated from Equation 1 using parameter values determined by White and Blum (1995) ($E_a = 59.4$ kJ mol^{-1}, $a = 0.456$, $T_0 = 5$ °C) peak at middle elevation sites and follow similar patterns to measured chemical weathering rates with changing elevation (Figure 7).

Discussion

Quantitative links between chemical weathering and erosion

Our data suggest linkages between rates of total chemical weathering and physical erosion in the Sierra Nevada (Figure 3a); previous authors have noted similar relationships across

**Table IV.** Rates of erosion and weathering

Sample	W_{soil}[a] (t km^{-2} y^{-1})	E[a] (t km^{-2} y^{-1})	W_{sap}[a] (t km^{-2} y^{-1})	W_{total}[a] (t km^{-2} y^{-1})	D[b] (t km^{-2} y^{-1})	Soil depth (cm)
Blasingame						
LD-0	0·0	66·2	75·4	75·4	141·5	6
LD-1	0·0	126·4	104·8	104·8	231·2	25
LD-2	24·4	80·5	34·4	58·7	139·3	27
LD-3	34·9	34·3	3·8	38·6	73·0	40
LD-4	38·5	54·8	27·5	66·1	120·8	45
LD-5	22·7	37·1	19·7	42·4	79·5	53
LD-6	5·5	45·7	53·4	58·9	104·6	75
Mean ± SE	18·0 ± 6·1	63·6 ± 12·1	45·6 ± 13·2	63·6 ± 8·4	127·1 ± 20·1	
Whitebark						
WB-0	13·0	57·5	39·5	52·5	110·0	53
WB-1	10·9	54·2	40·7	51·7	105·8	64
WB-2	0·0	34·2	43·1	43·1	77·4	70
WB-3	31·3	34·8	0·0	31·3	66·1	110
WB-4	5·1	35·1	25·4	30·6	65·6	75
WB-5	21·2	27·5	15·9	37·1	64·6	75
WB-6	11·4	23·6	6·4	17·8	41·4	60
WB-7	28·3	43·2	35·1	63·4	106·5	90
WB-8	5·7	34·3	18·0	23·7	57·9	80
Mean ± SE	14·1 ± 3·6	38·3 ± 3·8	24·9 ± 5·3	39·0 ± 5·0	77·3 ± 8·2	
Bretz Mill						
BM-2006-1	0·0	89·5	87·0	87·0	176·5	107
BM-2006-2	25·2	103·3	66·5	91·7	195·1	29
BM-2006-3	17·4	131·1	98·1	115·5	246·6	102
BM-2006-4	31·3	86·2	53·9	85·1	171·3	127
Mean ± SE	24·4 ± 7·9	104·4 ± 8·1	69·0 ± 10·6	93·4 ± 5·6	197·8 ± 13·3	
Providence Creek						
PC-1	4·2	131·8	158·0	162·2	294·0	80
PC-2	13·2	59·4	67·6	80·8	140·2	110
PC-2006-1	0·0	82·0	124·1	124·1	206·1	107
PC-2006-2	0·0	92·3	131·3	131·3	223·6	91
PC-2006-3	0·0	122·7	172·6	172·6	295·4	61
PC-2006-4	21·2	63·2	76·1	97·3	160·4	71
Mean ± S·E	6·4 ± 4·0	91·9 ± 13·4	121·6 ± 19·0	128·1 ± 15·9	220·0 ± 29·2	
Kaiser Road						
KR-1	n.d.	n.d.	4·8	n.d.	36·0	33
KR-2	n.d.	n.d.	0·0	n.d.	77·4	25
KR-2006-1	6·5	52·1	17·7	24·3	76·4	64
KR-2006-3	5·4	41·2	16·7	22·1	63·3	64
KR-2006-4	n.d.	n.d.	n.d.	n.d.	n.d.	64
Mean ± SE	6·0 ± 0·5	46·7 ± 5·4	9·8 ± 4·4	23·2 ± 1·1	63·3 ± 9·6	

[a] Calculated from CRN derived soil production rates (Table III) and zirconium concentrations (Table II), following Equations 10–12.
[b] Total denudation equals the sum of weathering (W_{total}) and erosion (E) rates.
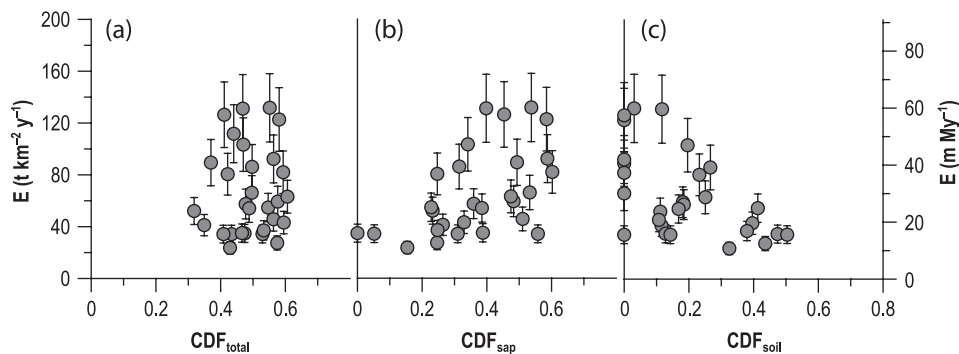
Figure 4. Physical erosion rates are plotted against CDF_{total} (a), CDF_{sap} (b) and CDF_{soil} (c). CDFs reflect fraction mass loss in the conversion of parent material (rock or saprolite) to weathered product (soil or saprolite). Total CDFs range between 40–60, suggesting very little variation at a hillslope scale or across the climate gradient. Physical erosion weakly increases with CDF_{sap} ($r^2 = 0.27$, $n = 29$) and decreases with CDF_{soil} ($r^2 = 0.30$, $n = 29$).
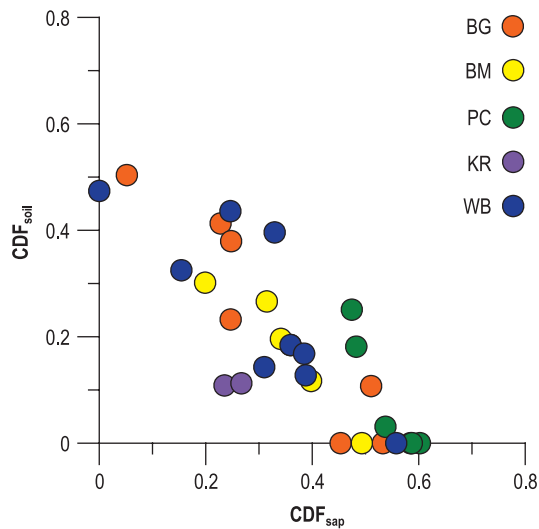
Figure 5. Chemical weathering intensity in soils and saprolites are inversely related at sampled climate zones BG [200 m elevation; pale gray (orange)], BM [1200 m elevation; light gray (yellow)], PC [1950 m elev; gray (green)], KR [2680 m elevation, dark gray (purple)] and WB [3000 m elevation; black (blue)]. The linear fit to these data is $CDF_{soil} = -0 \cdot 83(CDF_{sap}) + 0 \cdot 51$ ($r^2 = 0 \cdot 77$, $n = 27$). This relationship may suggest a tradeoff in chemical weathering in soils and saprolites, such that total weathering is roughly consistent across hillslopes. This figure is available in colour online at www.interscience.wiley.com/journal/espl

diverse upland landscapes (Figure 8), including the Canadian shield (Millot *et al.*, 2002), the mountains of New Zealand and the European Alps (West *et al.*, 2005), the Sierra Nevada (Riebe *et al.*, 2004), Puerto Rico (Riebe *et al.*, 2004) and Australia (Green *et al.*, 2006; Yoo *et al.*, 2007; Burke *et al.*, 2009). Here, we have the opportunity to examine the individual correlations between saprolite weathering, soil weathering, and physical erosion to gain a more mechanistic perspective of the underlying controls on erosion and weathering rates. Three important relationships emerge from our data.

First, physical erosion rates increase linearly with saprolite chemical weathering rates (Figure 3b). Although weathering and erosion rates are both calculated using CRN-derived soil production rates (Equations 10–12), this trend is not an artifact of the calculation for two reasons. (1) Calculations of chemical weathering and erosion rates are dependent on P_{soil} and zirconium in rock, saprolite and soil (Equations 10–12). If the correlation were driven by variations in P_{soil} alone, then ratios of zirconium concentrations would be constant across the landscape. This is not the case since zirconium concentrations (Table II) vary at both the hillslope scale and climate scale, and zirconium ratios (shown by CDFs in Figure 5) are also widely variable. (2) Physical erosion is positively correlated with both weathering rates and the intensity of saprolite weathering (shown by the CDF_{sap} in Figure 4b); suggesting a real connection between these two processes.

Second, although previous work suggested positive relationships between erosion and soil weathering, data presented here shows a weak inverse relationship between soil weathering intensity and erosion rate (Figure 4c). Soil zirconium concentrations and CDFs reveal mass losses by weathering during the conversion of saprolite to soil, but they can also reveal losses and gains that occur with subsequent downslope soil flux (Yoo *et al.*, 2007). Here, there are no systematic downslope variations in soil and saprolite zirconium or soil CDFs, suggesting that weathering during sediment transport is not capable of exerting a strong signal on these hillslopes.

Third, CDF_{sap} and CDF_{soil} are inversely related (Figure 5), indicating that saprolites that have experienced the greatest mass loss during their formation subsequently experience much less chemical weathering once they are converted to soil. In support of this, soils that are the most weathered are underlain by the least weathered saprolites. Because of the apparent tradeoff – or feedback – between saprolite and soil chemical weathering, the total weathering intensity across the study area is relatively stable (Figure 4a). Despite this consistency in CDF_{total}, the spatial variations in soil and saprolite CDFs across a single hillslope reveal further information about the nature of these feedbacks.

Correlations between weathering and erosion rates alone do not indicate mechanistic dependence; however, saprolite weathering appears to be an important control (Figures 3–5). Fletcher *et al.* (2006) proposed erosion may play an important role in influencing bedrock weathering by controlling saprolite thickness and maintaining oxygen diffusion; yet, we find few other mechanisms by which erosion may facilitate deep saprolite weathering. However, the chemical weathering of saprolite may promote faster rates of soil production and physical erosion by several mechanisms: increasing porosity, decreasing bedrock coherence, and creating material easily mobilized into soil and transported downslope. As noted earlier, intensely weathered saprolites restrict subsequent weathering in overlying soils. Therefore, despite favorable environmental conditions for weathering reactions in the soil (Banfield *et al.*, 1999), soil weathering may be hampered by the presence of clays and a lack of weatherable minerals. In contrast, saprolites with only minor chemical alteration provide a weatherable mineral suite to the soil. Fast physical erosion, driven by saprolite weathering, decreases mineral residence time within the soil column and on the hillslope, thereby reducing mineral interaction with water, biota and processes of chemical alteration.

While this study focuses primarily on rates and intensities of chemical weathering based on *in situ* [10]Be and zirconium concentrations, a new direction for quantifying these erosion and weathering feedbacks could include measurements of saprolite shear strength, clay concentrations, mineral specific weathering rates, and also a comparison of more traditional measurements of soil and saprolite character with weathering rates. Furthermore, it is unclear whether erosion and saprolite weathering remain positively correlated in highly weathered tropical environments, or whether intense saprolite weathering may reduce physical mobility of soil as clay concentrations and material cohesion increase (von Blanckenburg *et al.*, 2004). Regardless, the key finding here appears to be that saprolite weathering influences intensities and rates of erosion and weathering in overlying soil. In the next section we discuss the potential climate controls on these processes.

Erosion and weathering across a climate gradient

Modeled silica fluxes from Equation 1 predict higher weathering rates at middle elevations across this study area due to the combined effects of precipitation and temperature (Figure 7), in agreement with the pattern of measured total chemical weathering rates. At low elevations, high temperatures favor fast weathering reactions; however the low precipitation (33 cm y^{-1}) are likely unable to rapidly remove solutes, which limits chemical weathering. Although high elevation sites receive adequate precipitation, temperatures are low. Seasonality also inhibits weathering at all elevations: the bulk of precipitation arrives in the cool winter (and as snow at the highest elevations). Low chemical weathering rates observed at high elevation sites in this study are likely influenced by both cooler temperatures
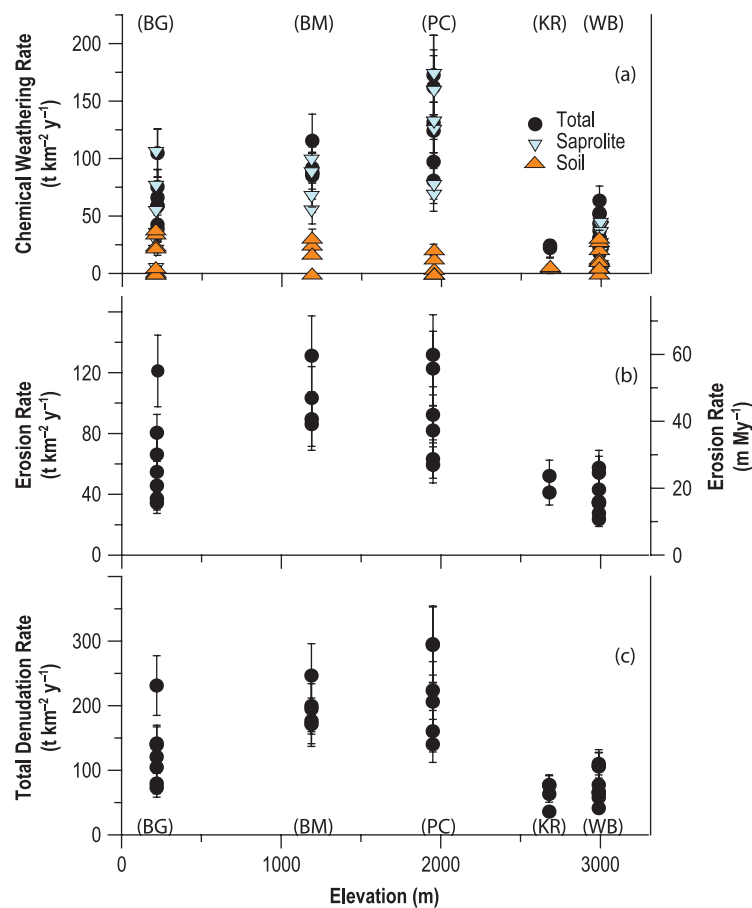
Figure 6. Chemical weathering rates (a) in soils and saprolites, physical erosion rates (b) and total denudation rates (c) show strong variation across the climate gradient, with the highest rates at middle elevation zones BM and PC. This figure is available in colour online at www.interscience.wiley.com/journal/espl
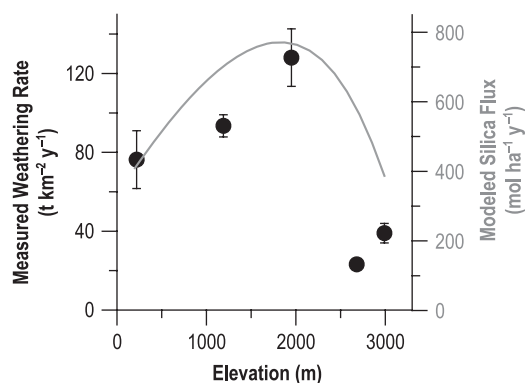
Figure 7. Modeling the coupled effects of temperature and precipitation on weathering. Silica fluxes (line) were modeled from Equation 1 using values of E_a and a_i parameterized by field data from White and Blum (1995) ($E_a = 59 \cdot 4$ kJ mol^{-1}, $a_i = 0 \cdot 456$, $T_0 = 5$ ºC). Measured average rates of chemical weathering (circles) follow similar patterns as modeled fluxes along the climate gradient. Error bars represent the standard error about the mean for total chemical weathering rates at each climate zone.

and rapid runoff associated with snowmelt (Dixon *et al.*, 2009).

The highest observed rates of soil chemical weathering occur at the middle elevation zone BM, corresponding to soils with high clay and secondary iron oxide concentrations. Across the same elevation transect Dahlgren *et al.* (1997) found that total soil clay increased from the low to mid-elevations (200–1600 m), the dropping precipitously at around 1600 m,

coincident with the average effective winter snow line. Similarly, soil weathering rates decreased roughly around this elevation, as PC, at elevation 1980 m, exhibits weathering rates similar to the highest elevations (Figure 6a). In contrast, saprolite weathering rates do not decrease across this elevation boundary: saprolite and total weathering rates at both BM and PC are high. Deep saprolite weathering at site PC may be shielded to some degree from low surface temperatures and frozen water conditions that retard soil weathering rates; instead, it may reflect insulated temperatures beneath meters to tens of meters of overlying material and moisture dynamics at the bedrock weathering front that could be decoupled from seasonal changes in surface precipitation.

Soil weathering rates are dependent on temperature and water availability, which are determined by climate, and on the availability of weatherable minerals, which is inherited from the underlying saprolite. Therefore, feedbacks between saprolite and soil weathering (Figure 5), discussed in the previous section, also modulate the influence of climate on these weathering rates. Similarly, climate control on erosion along the elevation transect is likely modulated by erosion-weathering coupling suggested in Figures 3 and 4. Together, this data suggests that climate influences soil transport rates through direct control on bedrock and soil chemical weathering.

Assumptions and implications of the mass balance models

With the advent of CRN approaches to the determination of soil production rates, the primary focus of most researchers
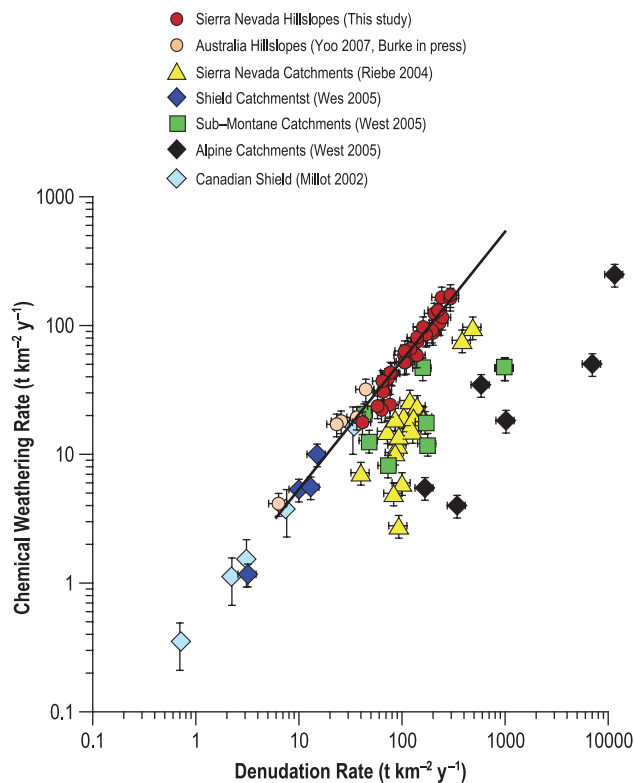
Figure 8. Rates of chemical weathering and denudation are tightly coupled across diverse landscapes (This study; Millot *et al.*, 2002; Riebe *et al.*, 2004; West *et al.*, 2005; Yoo *et al.*, 2005; Burke *et al.*, in press). Circles represent local CRN soil production rates, while triangles and diamonds represent catchment wide values determined either from CRN concentrations in river sands, or solute fluxes for rivers. We find greater scatter in erosion-weathering coupling at a catchment scale than at a local scale. Local rates from this study and Yoo et al. (2005) closely follow a power law function $W_{total} = 0.63(D)^{0.96}$ ($r^2 = 0.95$) that can be approximated by the linear function $W_{total} = 0.54(D)$. This figure is available in colour online at www.interscience.wiley.com/journal/espl

has been on the rates and patterns of landscape denudation, and on the nature of the soil production function. In these first-order investigations, the processes at the soil/bedrock interface (e.g. within saprolite) and their role in these patterns have been largely ignored, with the exception of a few studies (Green *et al.*, 2006; Burke *et al.*, 2007). Here, by adding new data detailing the chemical and physical patterns in soil and saprolite, our research supports the somewhat belated, but in retrospect obvious (e.g. Migon and Lidmar-Bergström, 2001), conclusion that factors and processes that control the breakdown of bedrock set the pace for subsequent biophysical and chemical processes that shape the landscape.

Similarly, the role of saprolite weathering has not been previously examined by using CRNs to derive denudation rates. CRN-based rates reflect near-surface lowering and soil production, as we discussed in a previous section, and do not record the deep weathering in saprolite due to the attenuation of CRN production with depth. We compare rates of weathering and erosion across the Sierra Nevada (Figures 9a–9e), calculated using equations derived from Riebe *et al.* (2003a), which assume that CRN-derived rates reflect total denudation, and the more expansive models in this paper. Calculated rates from the two mass balance approaches differ most when saprolite weathering is high, while sites with thin or poorly weathered saprolite are, as expected, well approximated by the Riebe

et al. (2003a) model. In particular, at Riebe's Sierran Sites, rock and saprolite zirconium concentrations were not statistically different, and saprolite weathering was therefore minor. It is unclear why there was little saprolite weathering at Riebe's sites, given the intensely weathered saprolites observed in this study. Boulder outcrops covered greater than 30% of some catchments (appendix to Riebe *et al.*, 2001b), further suggesting limited weathering. Possibly, the steep slopes in some of those catchments may reflect more rapid, tectonically driven incision (Riebe *et al.*, 2001b).

At sites sampled in this study, where saprolite weathering accounts for an average of 34 ± 3% (*n* = 32) of the total mass loss, the rates calculated by the two different methods diverge by up to a factor of three (Figure 9a). The calculated rates of soil weathering, total weathering, erosion and total denudation (Figures 9b–9e) are also higher in the adapted approach presented herein, such that the previous equations may significantly underestimate rates of mass loss. Thus, in order to gain a full measure of the total chemical weathering on a landscape, saprolite weathering must be included in the assessments.

The models used here require the key assumption that soil and saprolite thicknesses are locally constant over time. Steady state soil thickness, where soil production is balanced by soil loss from weathering and erosion, has been hypothesized for most soil-mantled landscapes, particularly those that reveal an inverse relationship between soil thickness and production rate (e.g. Heimsath *et al.*, 1997). If erosion exceeds soil production, then soils will thin to zero depth, while if soil production exceeds erosion then we should expect infinitely thick soils. The assumption of steady state saprolite thickness is not as widely accepted. Saprolite may not display a discrete thickness and can range from a thin, centimeter-thick mantle atop bedrock to upwards of tens of meters thick, suggesting that thickness may not be constant over time on all landscapes (e.g. Dethier and Lazarus, 2006). Saprolites may be residual from previous climate conditions (e.g. Oberlander, 1974); in this case it may be the intensity of past weathering and not the active weathering rate that influences erosion rates in overlying soil. Despite this, weathering and erosion may be linked by feedbacks that maintain a steady state saprolite thickness; Fletcher *et al.* (2006) used a spheroidal weathering model to show how the bedrock weathering front may propagate in step with the surface denudation rate due to oxygen diffusion into the saprolite. In the model of Riebe *et al.* (2003a), the assumptions of steady state soil and saprolite thicknesses are necessary to calculate any component of denudation. In the extended model here, the assumption of saprolite steady state thickness is only required when calculating rates of saprolite weathering (Equation 15).

Another key assumption in the use of mass balance models is the selection of a reference element. The immobility of an element depends on the chemical resistance of its host mineral and its chemical behavior in soil solutions. Zirconium commonly appears to meet both these criteria more strongly than related elements on the periodic table, such as titanium and cerium (Green *et al.*, 2006). Despite its conservative nature, the spatial variability of zirconium has not been well characterized in rock. Thus, we measured bedrock zirconium concentrations at each climate zone to account for variations in zircon distribution between different granitic lithologies. Further quantification of bedrock [Zr] variation at a hillslope scale was not possible in this study because outcropping bedrock was limited to a few emergent tors. Burke *et al.* (2009) quantified spatial variability in saprolite [Zr], and found coefficients of variation at a 4 m² scale range from 7% to 20%. We do not believe that geochemical variability strongly influences soil, saprolite or rock zirconium at our sites; if this were the case, it is highly
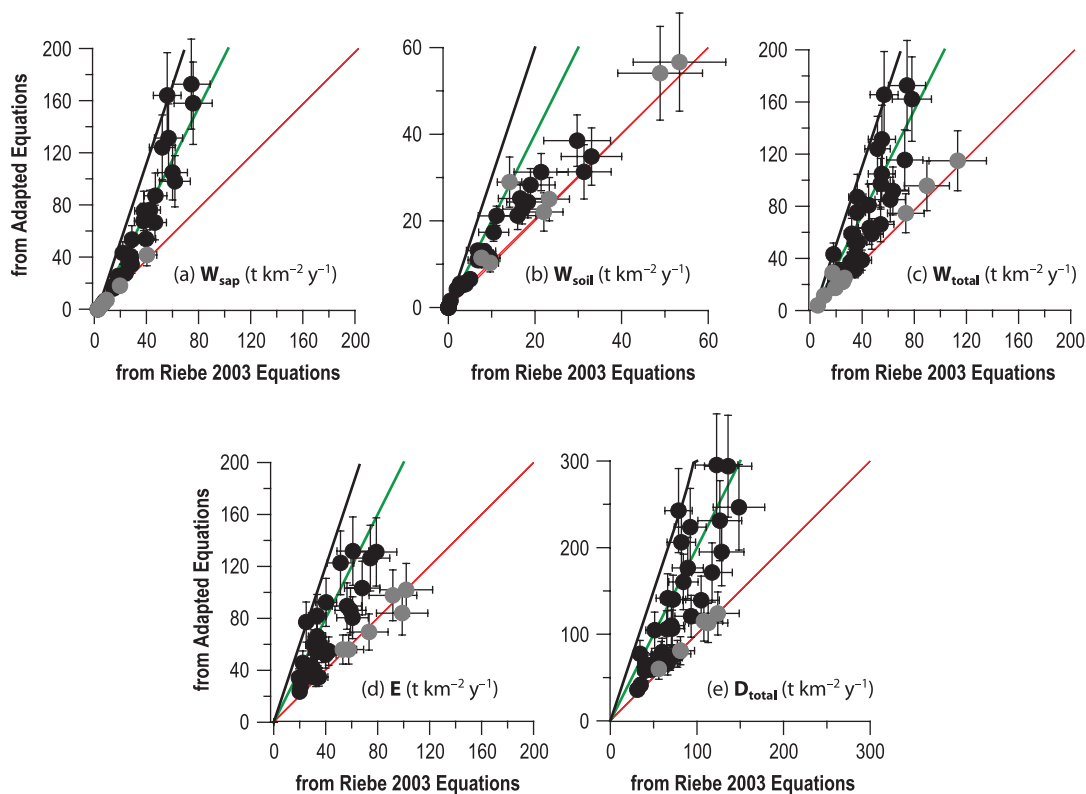
Figure 9. Units for both *x* and *y*-axes are in tons km^{-2} y^{-1}. Rates of saprolite chemical weathering (a), soil weathering (b), total weathering (c), physical erosion (d), and total denudation (e) calculated using the approach of Riebe *et al.* (2003a) (*x*-axis) and adapted equations presented in this study (*y*-axis). The approach by Riebe *et al.* (2003a) assumes CRN derived rates reflect total denudation, while the equations presented in this paper (Equations 15, 16 and 19) are derived assuming CRN derived rates reflect only soil production. Thin light gray (red), gray (green) and black lines represent 1:1, 2:1 and 3:1 lines respectively. The previous approach approximates rates of erosion and weathering on landscapes with minimal saprolite weathering, as in the case of data from Riebe *et al.* (2001b) (gray circles). On hillslopes examined in this study (black circles), with intensely weathered saprolites, the calculated rates from the two approaches vary by up to a factor of three indicating that the previous approach may dramatically underestimate rates of weathering, erosion and total denudation on landscapes mantled by saprolite. Axes are cropped to highlight variation in the two calculation methods, and some points may lie outside the range displayed. This figure is available in colour online at www.interscience.wiley.com/journal/espl

unlikely we would be able to discern the strong trends between chemical weathering and physical erosion rates, or between saprolite and soil CDFs.

Conclusions

The results of this study indicate that climate (combined effect of rain and temperature) exerts strong chemical and physical controls on landscape evolution in the Sierra Nevada. Rates of chemical weathering peak at middle elevation climate zones with moderate mean annual temperatures (12–9 °C) and precipitation (66–92 mm y^{-1}). Weathering at the low elevation climate zone is likely limited by low precipitation and decreased interaction between water and soils and saprolites, while weathering at high elevation is limited by a combination of cold temperatures and limited liquid water.

We show previously theorized, but unquantified, feedbacks between weathering and erosion that emerge when we account for weathering losses in both the soil and saprolite. Data from the Sierra Nevada indicate that saprolite weathering rates often exceed rates of weathering and erosion in the overlying soil. Physical erosion is fastest where rates of total and saprolite chemical weathering are the greatest. Furthermore, CDF data show an inverse relationship between the weathering intensity of soils and saprolites, indicating that intensely weathered saprolites are overlain by weakly weathered soils. Together these data suggest that climate controls landscape

evolution by its direct influence on weathering processes that remove primary minerals and increase material susceptibility to erosion. Furthermore, saprolite weathering exerts considerable influence on rates of erosion and weathering in the overlying soil, suggesting the saprolite system plays an important (e.g. Thomas, 1994), but previously under-quantified, role in landscape evolution.

References

Anderson SP, Dietrich WE Jr, Brimhall GH. 2002. Weathering profiles, mass-balance analysis, and rates of solute loss: linkages between weathering and erosion in a small, steep catchment. *Bulletin of the Geological Society of America* **114**: 1143–1158.

Balco G, Stone JO, Lifton NA, Dunai TJ. 2008. A complete and easily accessible means of calculating surface exposure ages or erosion rates from ^{10}Be and ^{26}Al measurements. *Quaternary Geochronology* **3**: 174–194.

Banfield JF, Barker WW, Welch SA, Taunton A. 1999. Biological

Impact on Mineral Dissolution: Application of the Lichen Model to Understanding Mineral Weathering in the Rhizosphere. *Proceedings of the National Academy of Sciences of the United States of America* **96**: 3404–3411.

Bateman PC, Busacca AJ. 1983. *Millerton Lake Quadrangle, West-central Sierra Nevada, California – Analytic Data*, US Geological Survey Professional Paper, vol. 1261. US Geological Survey: Reston, VA; 20.

Bateman PC, Lockwood JP. 1970. *Kaiser Peak Quadrangle, Central Sierra Nevada, California – Analytic Data*, US Geological Survey Professional Paper, vol. 644-C. US Geological Survey: Reston, VA.

Bateman PC, Lockwood JP. 1976. *Shaver Lake Quadrangle, West-central Sierra Nevada, California – Analytic Data*. US Geological Survey Professional Paper, vol. 774-D. US Geological Survey: Reston, VA.

Brimhall GH, Dietrich WE. 1987. Constitutive mass balance relations between chemical composition, volume, density, porosity, and strain in metasomatic hydrochemical systems: results on weathering and pedogenesis. *Geochimica et Cosmochimica Acta* **51**: 567–587.

Brimhall GH, Chadwick OA, Lewis CJ, Compston W, Williams IS, Danti KJ, Dietrich WE, Power ME, Hendricks D, Bratt J. 1992. Deformational mass transport and invasive processes in soil evolution. *Science* **255**: 695–702. DOI: 10.1126/science.255.5045.695

Büdel J. 1957. Die doppelten Einebnungsflächen in den feuchten Tropen. *Zeitschrift für Geomorphologie* **1**: 201–228.

Burke BC, Heimsath AM, White AF. 2007. Coupling chemical weathering with soil production across soil-mantled landscapes. *Earth Surface Processes and Landforms* **32**: 853–873.

Burke BC, Heimsath A, White AF, Bostick BC. 2009. Spatial variability of saprolite chemical weathering rates and intensities. *Geoderma*. In press.

Burke BC, Heimsath A, Dixon JL, Chappell J, Yoo K. 2009. Weathering the escarpment: chemical and physical rates and processes, southeastern Australia. *Earth Surface Processes and Landforms* **34**: 768–785. DOI: 10.1002/esp.1764

Buss HL, Brantley SL, Sak PB, White AF. 2004. Mineral dissolution at the grantie-saprolite interface. In *11th International Symposium on Water–Rock Interaction* 11, Wanty RB, Seal RRI (eds). Saratoga Springs, NH: Taylor and Francis; 819–823.

Buss HL, Sak PB, Webb SM, Brantley SL. 2008. Weathering of the Rio Blanco quartz diorite, Luquillo Mountains, Puerto Rico: coupling oxidation, dissolution, and fracturing. *Geochimica et Cosmochimica Acta* **72**: 4488–4507.

Cecil MR, Ducea MN, Reiners PW, Chase CG. 2006. Cenozoic exhumation of the northern Sierra Nevada, California, from (U-Th)/He thermochronology. *Geological Society of America Bulletin* **118**: 1481–1488.

Clark MK, Maheo G, Saleeby J, Farley KA. 2005. The non-equilibrium landscape of the southern Sierra Nevada, California. *GSA Today* **15**: 4.

Collins DBG, Bras RL, Tucker GE. 2004. Modeling the effects of vegetation-erosion coupling on landscape evolution. *Journal of Geophysical Research – Earth Surface* **109**: F03004. DOI: 10.1029/2003JF000028

Dahlgren RA, Boettinger JL, Huntington GL, Amundson RG. 1997. Soil development along an elevational transect in the western Sierra Nevada, California. *Geoderma* **78**: 207–236.

Dethier DP, Lazarus ED. 2006. Geomorphic inferences from regolith thickness, chemical denudation and CRN erosion rates near the glacial limit, Boulder Creek catchment and vicinity, Colorado. *Geomorphology* **75**: 384–399.

Dixon JL, Heimsath A, Kaste JM, Amundson R. 2009. Climate driven processes of hillslope weathering. *Geology*. In press.

Fletcher RC, Buss HL, Brantley SL. 2006. A spheroidal weathering model coupling porewater chemistry to soil thicknesses during steady-state denudation. *Earth and Planetary Science Letters* **244**: 444–457.

Frazier CS, Graham RC. 2000. Pedogenic transformation of fractured granitic bedrock, southern California. *Soil Science Society of America Journal* **64**: 2057–2069.

Green EG, Dietrich WE, Banfield JF. 2006. Quantification of chemical weathering rates across an actively eroding hillslope. *Earth and Planetary Science Letters* **242**: 155–169.

Hales TC, Roering JJ. 2007. Climatic controls on frost cracking and implications for the evolution of bedrock landscapes. *Journal of Geophysical Research* **112**: F02033. DOI: 10.1029/2006JF000616

Heimsath AM. 2006. Eroding the land: steady-state and stochastic rates and processes through a cosmogenic lens. *GSA Special Paper* **415**: 111–129. DOI: 10.1130/2006.2415(07)

Heimsath AM, Dietrich WE, Nishiizumi K, Finkel RC. 1997. The soil production function and landscape equilibrium. *Nature* **388**: 358–361.

Heimsath AM, Dietrich WE, Nishiizumi K, Finkel RC. 1999. Cosmogenic nuclides, topography, and the spatial variation of soil depth. *Geomorphology* **27**: 151–172.

Heimsath AM, Dietrich WE, Nishiizumi K, Finkel RC. 2001. Stochastic processes of soil production and transport: erosion rates, topographic variation, and cosmogenic nuclides in the Oregon Coast Range. *Earth Surface Processes and Landforms* **26**: 531–552.

House MA, Wernicke BP, Farley KA. 1998. Dating topography of the Sierra Nevada, California, using apatite (U-Th)/He ages. *Nature* **396**: 66–69.

Jacobson AD, Blum JD, Chamberlain CP, Craw D, Koons PO. 2003. Climatic and tectonic controls on chemical weathering in the New Zealand Southern Alps. *Geochimica et Cosmochimica Acta* **67**: 29–46.

Jenny H. 1941. *Factors of Soil Formation: A System of Quantitative Pedology*. McGraw-Hill: New York.

Lal D. 1991. Cosmic ray labeling of erosion surfaces: in situ nuclide production rates and erosion models. *Earth and Planetary Science Letters* **104**: 424–439.

Lebedeva MI, Fletcher RC, Balashov VN, Brantley SL. 2007. A reactive diffusion model describing transformation of bedrock to saprolite. *Chemical Geology* **244**: 624–645.

Lidmar-Bergström K. 1995. Relief and saprolites through time on the Baltic Shield. *Geomorphology* **12**: 45–61.

Migoń P, Alcántara-Ayala I. 2008. Weathering and landform development in a subtropical mountainous terrain, Veladero massif, Mexico. *Zeitschrift für Geomorphologie* **52**: 1–16.

Migoń P, Lidmar-Bergström K. 2001. Weathering mantles and their significance for geomorphological evolution of central and northern Europe since the Mesozoic. *Earth-Science Reviews* **56**: 285–324.

Millot R, Gaillardet J, Dupre B, Allegre CJ. 2002. The global control of silicate weathering rates and the coupling with physical erosion: new insights from rivers of the Canadian Shield. *Earth and Planetary Science Letters* **196**: 83–98.

Murphy SF, Brantley SL, Blum AE, White AF, Dong H. 1998. Chemical weathering in a tropical watershed, Luquillo Mountains, Puerto Rico: II. Rate and mechanism of biotite weathering. *Geochimica et Cosmochimica Acta* **62**: 227–243.

Nesbitt HW, Markovics G. 1997. Weathering of granodioritic crust, long-term storage of elements in weathering profiles, and petrogenesis of siliciclastic sediments. *Geochimica et Cosmochimica Acta* **61**: 1653.

Nugent MA, Brantley SL, Pantano CG, Maurice PA. 1998. The influence of natural mineral coatings on feldspar weathering. *Nature* **395**: 588–591.

Oberlander TM. 1974. Landscape inheritance and the pediment problem in the Mojave Desert of southern California. *American Journal of Science* **274**: 849–875.

Ollier CD. 1960. The inselbergs of Uganda. *Zeitschrift für Geomorphologie* **4**: 43–52.

Pavich MJ. 1986. Processes and rates of saprolite production and erosion on a foliated granitic rock of the Virginia piedmont. In *Rates of Chemical Weathering of Rocks and Minerals*, Colman SM, Dethier DP (eds). Academic Press: New York; 551–590.

Pavich MJ. 1990. Characteristics, origin, and residence time of saprolite and soil of the piedmont upland, Virginia, U.S.A., and model testing using cosmogenic 10Be. *Geochemistry of the Earth's Surface and of Mineral Formation 2nd International Symposium*, 12 July, Aix en Provence, France.

Phillips JD. 2005. Weathering instability and landscape evolution. *Geomorphology* **67**: 255–272.

Poage MA, Chamberlain CP. 2002. Stable isotopic evidence for a Pre-Middle Miocene rain shadow in the western Basin and Range:

implications for the paleotopography of the Sierra Nevada. *Tectonics* **21**: 1–10.

Price JR, Velbel MA, Patino LC. 2005. Rates and time scales of clay-mineral formation by weathering in saprolitic regoliths of the southern Appalachians from geochemical mass balance. *Geological Society of America Bulletin* **117**: 783–794.

Prism-Database. 2008. PRISM Group, Oregon State University. http://www.prismclimate.org [5 March 2008].

Riebe CS, Kirchner JW, Finkel RC. 2003a. Long-term rates of chemical weathering and physical erosion from cosmogenic nuclides and geochemical mass balance. *Geochimica et Cosmochimica Acta* **67**: 4411–4427.

Riebe CS, Kirchner JW, Finkel RC. 2003b. Sharp decrease in long-term chemical weathering rates along an altitudinal transect. *Earth and Planetary Science Letters* **6393**: 1–14.

Riebe CS, Kirchner JW, Finkel RC. 2004. Erosional and climatic effects on long-term chemical weathering rates in granitic landscapes spanning diverse climate regimes. *Earth and Planetary Science Letters* **224**: 547–562.

Riebe CS, Kirchner JW, Granger DE, Finkel RC. 2000. Erosional equilibrium and disequilibrium in the Sierra Nevada, inferred from cosmogenic Al and Be in alluvial sediment. *Geology* **28**: 803–806.

Riebe CS, Kirchner JW, Granger DE, Finkel RC. 2001a. Minimal climatic control on erosion rates in the Sierra Nevada, California. *Geology* **29**: 447–450.

Riebe CS, Kirchner JW, Granger DE, Finkel RC. 2001b. Strong tectonic and weak climatic control of long-term chemical weathering rates. *Geology* **29**: 511–514.

Small EE, Anderson RS. 1995. Geomorphically driven late Cenozoic rock uplift in the Sierra-Nevada, California. *Science* **270**: 277–280.

Stewart BW, Capo RC, Chadwick OA. 2001. Effects of rainfall on weathering rate, base cation provenance, and Sr isotope composition of Hawaiian soils. *Geochimica et Cosmochimica Acta* **65**: 1087–1099.

Stock GM, Anderson RS, Finkel RC. 2004. Pace of landscape evolution in the Sierra Nevada, California, revealed by cosmogenic dating of cave sediments. *Geology* **32**: 193–196.

Stolt MH, Baker JC. 2000. Quantitative comparison of soil and saprolite genesis; examples from the Virginia Blue Ridge and Piedmont (in Regolith in the Central and Southern Appalachians). *Southeastern Geology* **39**: 129–150.

Thomas MF. 1966. Some geomorphological implications of deep weathering patterns in crystalline rocks in Nigeria. *Transactions of the Institute of British Geographers* **40**: 173–191.

Thomas MF. 1994. *Geomorphology in the Tropics: A Study of Weathering and Denudation in Low Latitudes*. John Wiley & Sons: New York; 460 pp.

Trumbore SE, Chadwick OA, Amundson R. 1996. Rapid exchange between soil carbon and atmospheric carbon dioxide driven by temperature change. *Science* **272**: 393–396.

Tucker GE, Slingerland R. 1997. Drainage basin response to climate change. *Water Resources Research* **33**: 2031–2047.

von Blanckenburg F. 2006. The control mechanisms of erosion and weathering at basin scale from cosmogenic nuclides in river sediment. *Earth and Planetary Science Letters* **242**: 224.

von Blanckenburg F, Hewawasan T, Kubik *PW. 2004.* Cosmogenic nuclide evidence for low weathering and denudation in the wet, tropical highlands of Sri Lanka. *Journal of Geophysical Research* **109**: F03008. DOI: 10.1029/2003JF000049

West A, Galy A, Bickle M. 2005. Tectonic and climatic controls on silicate weathering. *Earth and Planetary Science Letters* **235**: 211–228.

White AF, Blum AE. 1995. Effects of climate on chemical weathering in watersheds. *Geochimica et Cosmochimica Acta* **59**: 1729–1747.

White AF, Brantley SL. 2003. The effect of time on the weathering of silicate minerals: why do weathering rates differ in the laboratory and field? *Chemical Geology* **202**: 479.

White AF, Blum AE, Bullen TD, Vivit DV, Schulz M, Fitzpatrick J. 1999. The effect of temperature on experimental and natural chemical weathering rates of granitoid rocks. *Geochimica et Cosmochimica Acta* **63**: 3277.

White AF, Bullen TD, Schulz MS, Blum AE, Huntington TG, Peters NE. 2001. Differential rates of feldspar weathering in granitic regoliths. *Geochimica et Cosmochimica Acta* **65**: 847.

White AF, Blum AE, Schulz MS, Vivit DV, Stonestrom DA, Larsen M, Murphy SF, Eberl D. 1998. Chemical weathering in a tropical watershed, Luquillo Mountains, Puerto Rico: I. Long-term versus short-term weathering fluxes. *Geochimica et Cosmochimica Acta* **62**: 209–226.

Yoo K, Amundson R, Heimsath AM, Dietrich WE. 2005. Process-based model linking pocket gopher (Thomomys bottae) activity to sediment transport and soil thickness. *Geology* **33**: 917–920.

Yoo K, Amundson R, Heimsath AM, Dietrich WE, Brimhall GH. 2007. Integration of geochemical mass balance with sediment transport to calculate rates of soil chemical weathering and transport on hillslopes. *Journal of Geophysical Research – Earth Surfaces* **112**: F02013. DOI: 10.1029/2005JF000402